

# Faraday Discussions

This paper is published as part of Faraday Discussions volume 144:  
Multiscale Modelling of Soft Matter

## Introductory Lecture

### Multiscale simulation of soft matter systems

Christine Peter and Kurt Kremer, *Faraday Discuss.*, 2010

DOI: [10.1039/b919800h](https://doi.org/10.1039/b919800h)

## Papers

### Fine-graining without coarse-graining: an easy and fast way to equilibrate dense polymer melts

Paola Carbone, Hossein Ali Karimi-Varzaneh and Florian Müller-Plathe, *Faraday Discuss.*, 2010

DOI: [10.1039/b902363a](https://doi.org/10.1039/b902363a)

### Systematic coarse-graining of molecular models by the Newton inversion method

Alexander Lyubartsev, Alexander Mirzoev, LiJun Chen and Aatto Laaksonen, *Faraday Discuss.*, 2010

DOI: [10.1039/b901511f](https://doi.org/10.1039/b901511f)

### Mesoscale modelling of polyelectrolyte electrophoresis

Kai Grass and Christian Holm, *Faraday Discuss.*, 2010

DOI: [10.1039/b902011j](https://doi.org/10.1039/b902011j)

### Kinetic Monte Carlo simulations of flow-induced nucleation in polymer melts

Richard S. Graham and Peter D. Olmsted, *Faraday Discuss.*, 2010

DOI: [10.1039/b901606f](https://doi.org/10.1039/b901606f)

## Discussion

### General discussion

*Faraday Discuss.*, 2010

DOI: [10.1039/b917706j](https://doi.org/10.1039/b917706j)

## Papers

### Simulations of theoretically informed coarse grain models of polymeric systems

François A. Detcheverry, Darin Q. Pike, Paul F. Nealey, Marcus Müller and Juan J. de Pablo, *Faraday Discuss.*, 2010

DOI: [10.1039/b902283j](https://doi.org/10.1039/b902283j)

### A simple coarse-grained model for self-assembling silk-like protein fibers

Marieke Schor, Bernd Ensing and Peter G. Bolhuis, *Faraday Discuss.*, 2010

DOI: [10.1039/b901608b](https://doi.org/10.1039/b901608b)

### Phase behavior of low-functionality, telechelic star block copolymers

Federica Lo Verso, Athanassios Z. Panagiotopoulos and Christos N. Likos, *Faraday Discuss.*, 2010

DOI: [10.1039/b905073f](https://doi.org/10.1039/b905073f)

### Mesosopic modelling of colloids in chiral nematics

Miha Ravnik, Gareth P. Alexander, Julia M. Yeomans and Slobodan Zumer, *Faraday Discuss.*, 2010

DOI: [10.1039/b908676e](https://doi.org/10.1039/b908676e)

### A molecular level simulation of a twisted nematic cell

Matteo Ricci, Marco Mazzeo, Roberto Berardi, Paolo Pasini and Claudio Zannoni, *Faraday Discuss.*, 2010

DOI: [10.1039/b901784d](https://doi.org/10.1039/b901784d)

### Lyotropic self-assembly mechanism of T-shaped polyphilic molecules

Andrew J. Crane and Erich A. Müller, *Faraday Discuss.*, 2010

DOI: [10.1039/b901601e](https://doi.org/10.1039/b901601e)

## Discussion

### General discussion

*Faraday Discuss.*, 2010

DOI: [10.1039/b917708f](https://doi.org/10.1039/b917708f)

## Papers

### Coarse-grained simulations of charge, current and flow in heterogeneous media

Benjamin Rotenberg, Ignacio Pagonabarraga and Daan Frenkel, *Faraday Discuss.*, 2010

DOI: [10.1039/b901553a](https://doi.org/10.1039/b901553a)

### Multi-particle collision dynamics simulations of sedimenting colloidal dispersions in confinement

Adam Wysocki, C. Patrick Royall, Roland G. Winkler, Gerhard Gompper, Hajime Tanaka, Alfons van Blaaderen and Hartmut Löwen, *Faraday Discuss.*, 2010

DOI: [10.1039/b901640f](https://doi.org/10.1039/b901640f)

### Can the isotropic-smectic transition of colloidal hard rods occur via nucleation and growth?

Alejandro Cuetos, Eduardo Sanz and Marjolein Dijkstra, *Faraday Discuss.*, 2010

DOI: [10.1039/b901594a](https://doi.org/10.1039/b901594a)

### Multi-scale simulation of asphaltene aggregation and deposition in capillary flow

Edo S. Boek, Thomas F. Headen and Johan T. Padding, *Faraday Discuss.*, 2010

DOI: [10.1039/b902305b](https://doi.org/10.1039/b902305b)

### The crossover from single file to Fickian diffusion

Jimaan Sané, Johan T. Padding and Ard A. Louis, *Faraday Discuss.*, 2010

DOI: [10.1039/b905378f](https://doi.org/10.1039/b905378f)

### Mori–Zwanzig formalism as a practical computational tool

Carmen Hijón, Pep Español, Eric Vanden-Eijnden and Rafael Delgado-Buscalioni, *Faraday Discuss.*, 2010

DOI: [10.1039/b902479b](https://doi.org/10.1039/b902479b)

## Discussion

### General discussion

*Faraday Discuss.*, 2010

DOI: [10.1039/b917709b](https://doi.org/10.1039/b917709b)

## Papers

### Hierarchical coarse-graining strategy for protein-membrane systems to access mesoscopic scales

Gary S. Ayton, Edward Lyman and Gregory A. Voth, *Faraday Discuss.*, 2010

DOI: [10.1039/b901996k](https://doi.org/10.1039/b901996k)

### Towards an understanding of membrane-mediated protein–protein interactions

Marianna Yiannourakou, Luca Marsella, Frédérick de Meyer and Berend Smit, *Faraday Discuss.*, 2010

DOI: [10.1039/b902190f](https://doi.org/10.1039/b902190f)

### Measuring excess free energies of self-assembled membrane structures

Yuki Norizoe, Kostas Ch. Daoulas and Marcus Müller, *Faraday Discuss.*, 2010

DOI: [10.1039/b901657k](https://doi.org/10.1039/b901657k)

### Lateral pressure profiles in lipid monolayers

Svetlana Baoukina, Siewert J. Marrink and D. Peter Tieleman, *Faraday Discuss.*, 2010

DOI: [10.1039/b905647e](https://doi.org/10.1039/b905647e)

### Concerted diffusion of lipids in raft-like membranes

Touko Apajalahti, Perttu Niemelä, Praveen Nedumpully Govindan, Markus S. Miettinen, Emppu Salonen, Siewert-Jan Marrink and Ilpo Vattulainen, *Faraday Discuss.*, 2010

DOI: [10.1039/b901487j](https://doi.org/10.1039/b901487j)

### Membrane poration by antimicrobial peptides combining atomistic and coarse-grained descriptions

Andrzej J. Rzepiela, Durba Sengupta, Nicolae Goga and Siewert J. Marrink, *Faraday Discuss.*, 2010

DOI: [10.1039/b901615e](https://doi.org/10.1039/b901615e)

## Discussion

### General discussion

*Faraday Discuss.*, 2010

DOI: [10.1039/b917710h](https://doi.org/10.1039/b917710h)

## Concluding remarks

### Concluding remarks

Herman J. C. Berendsen, *Faraday Discuss.*, 2010

DOI: [10.1039/b917077b](https://doi.org/10.1039/b917077b)

# Can the isotropic-smectic transition of colloidal hard rods occur *via* nucleation and growth?

Alejandro Cuetos,<sup>†</sup> Eduardo Sanz,<sup>‡</sup> and Marjolein Dijkstra\*

Received 28th January 2009, Accepted 27th February 2009

First published as an Advance Article on the web 21st August 2009

DOI: 10.1039/b901594a

We investigate the isotropic-to-smectic transformation in a fluid of colloidal hard rods using computer simulations. At high supersaturation, we observe spinodal decomposition: many small clusters are formed at the initial stage of the phase transformation, which form a percolating network that eventually transforms into a stable bulk smectic phase. At low supersaturation, we find that nucleation and growth of the smectic phase is hampered by the pre-smectic ordering in the supersaturated isotropic fluid phase. As the system evolves mainly *via* cooperative motion of these smectic domains, the diffusion and attachment of single particles to the nucleation site is largely hindered.

## 1 Introduction

The interest in liquid crystalline phases is driven by their great technological potential, but also originates from a fundamental point of view. While the mechanisms that control the stability of the liquid crystalline phases are well-known, the transformation between the different mesophases with positional and orientational ordering is still poorly understood. For instance, the smectic phase is a liquid crystalline state of matter in which elongated particles, such as molecules, colloids, fibers, nanotubes, form parallel stacks of fluid-like layers. The formation of a smectic phase and the nature of the transient structures (clusters, nuclei, droplets) are, however, still unknown. When spherical particles nucleate, the clusters that form, tend to be spherical: *e.g.* the existence of gas-bubbles in a superheated liquid,<sup>1</sup> liquid droplets in a supersaturated gas,<sup>2</sup> or crystallites in an undercooled liquid<sup>3,4</sup> are undisputed transient structures. However, there seems to be no analogue for smectic clusters where both positional and orientational order plays a role and where anisotropic clusters may be formed: simple transient smectic droplets have to the best of our knowledge never been observed.

For instance, a simulation study on the crystal nucleation in fluids of short hard rods shows that the growth of a crystal starts with the formation of a single crystalline membrane with hexagonal order. Subsequently, the growth of the crystal is hampered by rods that are aligned parallel to the bottom and top surface of the crystallite: the surface poisons itself and hence prevents its own growth.<sup>5-7</sup> Consequently, the free energy increases monotonically with cluster size and never crosses a nucleation barrier beyond which the clusters grow spontaneously.

---

*Soft Condensed Matter Group, Debye Institute for NanoMaterials Science, Utrecht University, Princetonplein 5, 3584 CC Utrecht, The Netherlands. E-mail: m.dijkstra@uu.nl*

<sup>†</sup> Present address: Departamento de Física Aplicada, Universidad de Almería, 04020 Almería, Spain. E-mail: E-mail: acuetos@ual.es

<sup>‡</sup> Present address: SUPA, School of Physics and Astronomy, University of Edinburgh, Mayfield Road Edinburgh, UK. E-mail: E-mail: esanz@ph.ed.ac.uk

---

In addition, very intriguing structures have been observed by Dogic and Fraden in experiments on suspensions of rod-like virus particles and non-adsorbing polymer.<sup>8,9</sup> They observed a fascinating rich phenomenology with novel and interesting metastable structures depending on the polymer concentration, like spindle-shaped nematic droplets, filaments, surface-induced smectic phases on the surface of metastable nematic droplets, individual smectic membranes winding off from tactoids as twisted ribbons, but they never observed simple smectic droplets.<sup>8,9</sup> In addition, the kinetics of the isotropic-to-smectic transformation has also been studied in experiments on attractive  $\beta$ -FeOOH rod suspensions as a function of the aspect ratio, and again no smectic droplets have been observed.<sup>10</sup>

This should be contrasted with the isotropic-to-nematic (I–N) transition where only orientational order plays a role. The (existence of a) crossover between the nucleation and growth regime with a spinodal decomposition regime has been investigated experimentally as a function of supersaturation in systems of colloidal rods,<sup>11</sup> solutions of F-actin<sup>12</sup> or dispersions of rod-like viruses under shear conditions.<sup>13</sup> The location of the isotropic-nematic spinodal have been determined using Brownian dynamics simulations in fluids of hard rods for various aspect ratios.<sup>14</sup> In addition, the structure and the shape of the transient clusters during the isotropic-to-nematic transition have been well-studied, and spindle-shaped elongated nematic droplets, called tactoids, have been observed experimentally.<sup>12,15,16</sup> The shape and the nematic director field of tactoids have been described theoretically and different morphologies of the nematic tactoids have been predicted as a function of the interfacial tension, the anchoring strength, and the bulk elasticity.<sup>17</sup> Very recently, we have studied the isotropic-to-nematic transition in a fluid of hard spherocylinders and in a mixture of rods and non-adsorbing polymer.<sup>18,19</sup> To study the transformation from the isotropic-to-nematic phase, we introduced a new cluster criterion that enabled us to differentiate the nematic clusters from an isotropic fluid phase. Applying this criterion in Monte Carlo simulations, we found at high supersaturation spinodal decomposition, and at low supersaturation, we observed nucleation and growth. We determined the height of the nucleation barrier and we studied the shape and the structure of the cluster as a function of its size. We found that the clusters have an ellipsoidal symmetry with an aspect ratio of about 1.6 and a homogeneous nematic director field. Subsequently, we have explored the validity of classical nucleation theory (CNT) in fluids of hard rods in a mixture of rods and non-adsorbing polymer.<sup>19</sup> Although many questions remain to be answered for the isotropic-to-nematic transformation, *e.g.* on the nontrivial density and order parameter profiles inside the droplets, it is well-accepted by now that the transformation occurs *via* the formation of anisotropic nematic clusters at sufficiently low supersaturations.

In this paper, we investigate the isotropic-to-smectic transformation in a fluid of hard spherocylinders using computer simulations. We investigate whether the transformation proceeds *via* nucleation and growth or *via* spinodal decomposition, and what the shape and structure is of the transient structures along the transition. In addition, we like to investigate whether the growth of the smectic phase is also hampered by self-poisoning as was observed for the isotropic-to-crystal nucleation of short hard rods.<sup>5</sup> We also like to investigate whether the nucleation of the smectic can proceed in multiple steps in which the nucleation starts with the formation of a single layer, and subsequently additional layers are nucleated on top of this layer. The nucleation of additional layers do have their own nucleation barrier, and hence the free energy of formation of a multilayer stacked smectic/crystalline phase consists of a sequence of maxima and minima as was predicted theoretically by Frenkel and Schilling.<sup>7</sup> Finally, we study whether the isotropic-to-smectic transition proceeds *via* nematic tactoids as has been observed experimentally.<sup>8,9</sup>

This paper is arranged as follows. In Section II, we describe the simulation techniques and the model. In section III, we present the results, while in Section IV, we finish with some conclusions and final remarks.

## 2 Model and simulation method

We study the isotropic-to-smectic (I–Sm) transformation in a suspension of colloidal hard rods. We model the suspension as a fluid of hard spherocylinders (HSC) with diameter  $\sigma$  and length  $L$ . In this model, the pair potential of two rods is given by

$$U_{\text{HSC}}(\mathbf{r}, \hat{\mathbf{u}}_i, \hat{\mathbf{u}}_j) = \begin{cases} \infty & d_m \leq \sigma \\ 0 & d_m > \sigma \end{cases} \quad (1)$$

where  $d_m$  is the minimum distance between two line segments of length  $L$  with orientations  $\hat{\mathbf{u}}_i$  and  $\hat{\mathbf{u}}_j$ , and relative distance vector  $\mathbf{r}$ . This model has been extensively studied in the past, and its phase diagram is well known as a function of the length-to-diameter ratio of the rods.<sup>20,21</sup> In this paper, we focus on particles with a length-to-diameter ratio of  $L^* = L/\sigma = 3.4$ . For  $L^* = 3.4$ , the system exhibits an isotropic (I), smectic A (Sm) and a crystal (X) phase, while the nematic phase is unstable for this elongation. The I–Sm transition occurs at coexistence pressure  $P^*_{\text{ISM}} = 2.818$ , where the reduced pressure is defined as  $P^* = \beta P \sigma^3$  with  $\beta = 1/k_{\text{B}}T$ ,  $k_{\text{B}}$  Boltzmann's constant, and  $T$  the temperature. The packing fractions of the coexisting isotropic and smectic phase are  $\eta_{\text{I}} = 0.492$  and  $\eta_{\text{Sm}} = 0.552$ , respectively.<sup>20</sup> Here, we define the packing fraction  $\eta = \rho v_o$ , with  $\rho = N/V$  the number density and  $v_o$  the volume of the rods.

To study the transformation of the isotropic to smectic phase, we perform either standard Monte Carlo simulation in the isobaric-isothermal ensemble, *i.e.*, the number of particles, pressure and temperature are kept fixed (NPT-MC simulations), or we employ the umbrella-sampling method in the isobaric-isothermal ensemble. We perform our simulations in a rectangular box with periodic boundary conditions and we use  $N = 8649$  particles. We do not expect appreciable finite-size effects for this system size. The acceptance ratios are kept within 30–40% for the rotational and translational moves of the particles, and within 20–30% for the attempts to change the volume of the box. Box volume changes are attempted by randomly changing the length of each side of the box independently.

We first employ the NPT-MC simulations to equilibrate states in both the isotropic and the smectic phase. We note, however, that our results deviate slightly from those in ref. 20. We find after long equilibration that the packing fraction of the isotropic phase at the coexistence pressure  $P^* = 2.818$  reported in ref. 20 is similar to their value, *i.e.*,  $\eta = 0.492 \pm 0.001$ . However, we find that our value for the packing fraction of the smectic phase, *i.e.*,  $\eta = 0.535 \pm 0.001$ , at this pressure is slightly lower than in ref. 20. This deviation in the density of the smectic phase can be explained by the fact that our system can relax its stress as the sides of the simulation box have been changed independently in the volume changes.

At high supersaturations, we employ standard MC-NPT simulations to study the I–Sm transformation. We first equilibrate an isotropic fluid phase at the coexistence pressure, and subsequently quench the system to a pressure beyond coexistence and we monitor different order parameters that provide us with information about the intermediate states during the I–Sm transformation. At low supersaturation, *i.e.* at pressures slightly higher than the coexistence pressure, the free energy to form a critical cluster is very high, and hence, a spontaneous fluctuation that brings the system to the top of the free energy barrier, which is needed for spontaneous growth of the cluster, is extremely rare. Standard MC simulations can therefore not be used to study nucleation at low supersaturations. In order to study nucleation at low supersaturations, we employ umbrella sampling that allows us to bias the sampling to configurations that contain clusters with a certain size. We use the number of particles  $n$  in the largest nematic cluster as an order parameter. Following the methodology described in ref. 2, we employ the biasing potential  $W$ :

$$W(n(\mathbf{r}^N, \mathbf{u}^N)) = 1/2\kappa_n[n(\mathbf{r}^N, \mathbf{u}^N) - n_0]^2 \quad (2)$$

Here the constant  $\kappa_n$  and  $n_0$  determine the width and location of the range of cluster sizes that is sampled. Typical values for  $\kappa_n$  are in the range of 0.13–0.17. In our simulations, we apply the biasing potential only after trajectories of 10 MC cycles, as the computation of the size of the biggest cluster is very time consuming.

If  $\langle N_n \rangle$  denotes the average number of clusters with  $n$  particles, one can determine the probability distribution  $P(n) = \langle N_n \rangle / N$ , with  $N$  the total number of particles. The Gibbs free energy  $\Delta G(n)$  for the formation of a cluster of size  $n$  is then determined by:

$$\Delta G(n) = -k_B T \ln P(n) \quad (3)$$

When  $\Delta G(n)$  is at a maximum, the cluster at the top of the nucleation barrier is defined as the critical cluster. Clusters with a size larger than that of the critical cluster (postcritical clusters) will spontaneously grow and will eventually form the stable smectic phase in order to minimize the free energy, while clusters smaller than the critical cluster will shrink spontaneously. We employ the umbrella sampling technique to calculate the nucleation barrier. In addition, we use this technique to stabilize critical, precritical and postcritical clusters to study the internal structure and shape of these intermediate structures. In order to bias the sampling to configurations that contain clusters with a certain size, we need a cluster criterion that is able to identify the smectic clusters from the isotropic fluid phase. Recently, we developed a cluster criterion that enables us to distinguish the nematic clusters from the isotropic fluid phase. Here, we apply the same cluster criterion to identify the orientationally ordered clusters from the isotropic, orientationally disordered fluid phase. In the cluster criterion, we first make a distinction between particles that have a orientationally ordered and an isotropic environment. Particle  $i$  is orientationally ordered if its local environment has an orientational order significantly larger than in the isotropic phase. The local environment of particle  $i$  is defined by all particles  $j$  with a surface-to-surface distance  $\rho_{ij} \leq 1.5\sigma$ , *i.e.*, such that it is not only defined by the nearest neighbors, but also by the next-nearest neighbors, thereby taking advantage of the long-ranged orientational order in the nematic/smectic phase. The local orientational order of particle  $i$  is defined by

$$S(i) = \frac{1}{n_i} \sum_{j=1}^{n_i} \left( \frac{3}{2} |\mathbf{u}_j \cdot \mathbf{u}_i|^2 - \frac{1}{2} \right) \quad (4)$$

where  $\mathbf{u}_j$  is the unit orientation vector of particle  $j$  and  $n_i$  the number of particles with  $\rho_{ij} \leq 1.5\sigma$ . We have adopted the cluster criterion that particle  $i$  is orientationally ordered if  $S(i) > K_1$ , where  $K_1$  is a threshold value that has to be optimized for each model. After identifying the orientationally ordered particles in the system, we determine the smectic cluster with the criterion that two particles  $i$  and  $j$  belong to the same cluster if  $\rho_{ij} < 0.5\sigma$  and  $|\mathbf{u}_i \cdot \mathbf{u}_j| > K_2$ , with  $K_2$  another adjustable threshold value. In contrast with the first step of our cluster criterion, we consider only the first neighbors. In our previous simulation study of the I–N transition in a fluid of hard spherocylinders, we have chosen  $K_1 = 0.4$  and  $K_2 = 0.85$ . In the sequel of this paper, we denote this criterion as C1. The C1 criterion yields valuable information about the structural properties of the intermediate states observed during the I–Sm transition. However, for large cluster sizes and high supersaturations, these threshold values are not optimized to distinguish the smectic clusters from the isotropic fluid phase. We have performed several trial runs to optimize the threshold values and we have chosen  $K_1 = 0.5$  and  $K_2 = 0.95$ , which will be referred to as the C2 criterion. With this choice of parameters, we hardly find any smectic clusters in the coexisting isotropic fluid phase, *i.e.*, only clusters with  $n < 20$  particles are found. On the other

---

hand, more than 95% of the particles belong to an unique smectic cluster in the coexisting smectic phase. We wish to make several comments here: (i) the present criterion to distinguish smectic clusters from the isotropic phase is similar to the nematic cluster criterion used previously.<sup>18,19</sup> In fact, our cluster criteria do not make a distinction between nematic- or smectic-like particles, but only differentiate particles with a high local orientational order from particles with an isotropic environment. Therefore, the criterion does not bias the sampling towards cluster with a certain structure, *e.g.* nematic, smectic, or crystalline clusters. (ii) Our cluster criterion deviates from the criterion proposed by Schilling and Frenkel,<sup>5,6</sup> who used their criterion to study the isotropic-to-solid transition in a fluid of hard spherocylinders with elongation  $L^* = 2$ . In their criterion, two particles belong to the same cluster if the surface-to-surface distance between two rods is smaller than  $0.5\sigma$  and the absolute value of the dot product of the two unit vectors that define the orientations of the rods is larger than 0.995. However, this criterion cannot be used for the elongation of interest in this work, since only 50% of the particles in the coexisting smectic state belong to the smectic phase.

To analyze the results we employ techniques that are frequently used in liquid crystal studies. For example, we monitor the orientational order in a cluster or in the whole system using the standard nematic order parameter  $S$ . The nematic order parameter is defined by the largest eigenvalue of the standard  $3 \times 3$  nematic order parameter tensor. The corresponding eigenvector defines the preferred orientation of the particles, which defines the nematic director  $\mathbf{n}$ . To study the structure of the clusters we calculate the density  $\rho^*(z, r)$  at distance  $z$  from the center-of-mass of the clusters parallel to the nematic director of the clusters and distance  $r$  perpendicular to the nematic director of the clusters. In order to study the orientational order inside the cluster, we define a local orientational order parameter by averaging the second Legendre polynomial,  $S(z, r) = \langle 3/2|\mathbf{u}_i(z, r) \cdot \mathbf{n}|^2 - 1/2 \rangle$ , for orientationally ordered (smectic) and isotropic particles. Here  $\mathbf{n}$  is the nematic director calculated using only the particles that belong to the smectic cluster. In our calculations of the density and nematic order parameter profiles, we consider all the particles in the system.

### 3 Results

We study the I–Sm transformation using Monte Carlo simulations as a function of supersaturation. To this end, we first equilibrate an isotropic fluid phase of a fluid of hard spherocylinders with  $L^* = 3.4$  at bulk coexistence ( $P^* = 2.828$ ,  $\eta = 0.495 \pm 0.001$ ). When the system is well equilibrated, we increment the pressure, and we investigate at which pressure the I–Sm transition occurs spontaneously. We find that the isotropic phase transforms spontaneously into a smectic phase at  $P^* \geq 3.1$ . When we compress an isotropic fluid phase at  $P^* = 3.1$  using NPT-MC simulations, we find that the density of the system increases gradually and that the system is unstable. Phase separation sets in immediately after compressing, as many small clusters appear in the system in the initial stage of the phase separation. These clusters coalesce and form an interconnected cluster (see Fig. 1). The size and the nematic order of this interconnected cluster grow gradually until the whole system is transformed into a single smectic cluster in the final stage of the transformation. These features are characteristic of spinodal decomposition and we conclude that at this supersaturation the system is in the spinodal regime. Fig. 2 presents the evolution of the size of the largest cluster in the system, according to the C1 and C2 cluster criteria (bottom panel). The global order parameter of the whole system as well as the nematic order parameter of the biggest cluster according to both cluster criteria are presented in the top panel of Fig. 2. From this figure, we clearly observe how the system evolves gradually from a state without any orientational order, *i.e.*, the global

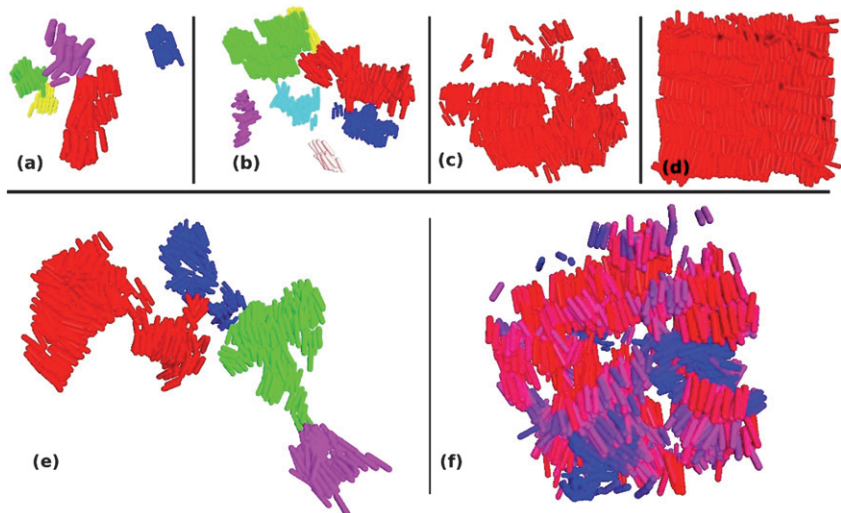


**Fig. 1** Typical intermediate configurations of clusters in the I–Sm transformation of a HSC fluid with  $L^* = 3.4$  as described in Fig. 2 using the C2 cluster criterion. (a) Clusters of 64 (red), 44 (green), 28 (blue), 20 (yellow) and 18 (magenta) particles are formed simultaneously. The packing fraction of the system is  $\eta = 0.500$  here. (b) Many clusters observed simultaneously in a configuration with  $\eta = 0.513$ . The size of the clusters is 238 particles (red), 209 (green), 118 (blue), 88 (yellow), 77 (cyan), 44 (magenta) and 24 (light pink). (c) In a later stage, when  $\eta = 0.518$ , the clusters coalesce and form a bigger cluster of 1587 particles. (d) In the final stage, the systems transform into a bulk Smectic A phase with a packing fraction of  $\eta = 0.550$ . (e) Same configuration as in (a) but now analyzed by using the C1 cluster criterion. We now observe clusters with 375 particles (red), 257 (green), 132 (blue) and 89 (green). (f) Same configuration as in (b), but analyzed using the C1 cluster criterion. An open, interconnected labyrinth-like structure of 2228 particles is found. The red particles have an orientation close to the nematic director  $\mathbf{n}$  of the cluster, while the blue particles are perpendicular to  $\mathbf{n}$ .

nematic order parameter  $S$  is close to zero, to a state with a high orientational order, *i.e.*,  $S$  close to unity. From Fig. 2, we observe that the global nematic order parameter is clearly correlated with the size of the biggest cluster in the system as detected by both cluster criteria. This should be contrasted with the nematic order parameter of the biggest cluster, which display a non-monotonous behavior during the transition. We can detect basically two regimes. In the initial stage of the phase separation, the nematic order parameter of the biggest cluster shows an irregular behavior with large and rapid oscillations around an averaged value, while in a later stage these oscillations almost disappear. In the final stage, the nematic order parameter of the biggest cluster shows a slight increase to a value, that is slightly higher than that of the global nematic order parameter. The trends as described above do not depend strongly on the C1 or the C2 cluster criteria. However, we do find some remarkable differences. First, we observe that the clusters already start to grow at  $0.5 \times 10^6$  MC cycles according to the C1 cluster criterion, while according to the C2 cluster criterion the clusters start to grow much later, at about  $1.5 \times 10^6$  MC cycles. At this stage, the C1 cluster criterion detects clusters of about 2000 particles. The C1 cluster criterion has been used to study the I–N transition<sup>18,19</sup> and is less strict than the C2 cluster criterion. Second, we observe from Fig. 2 that the nematic order parameter of the biggest cluster according to the C1 cluster criterion is very noisy in the initial stage of the transformation, decreases monotonically with time, and shows a minimum at about the same stage when the clusters start to grow according to the C2 cluster criterion. Subsequently, the nematic order parameter of the biggest cluster starts to grow till a maximum value is reached. In order to explain the trends observed in Fig. 2, we analyze the clusters observed during the transformation

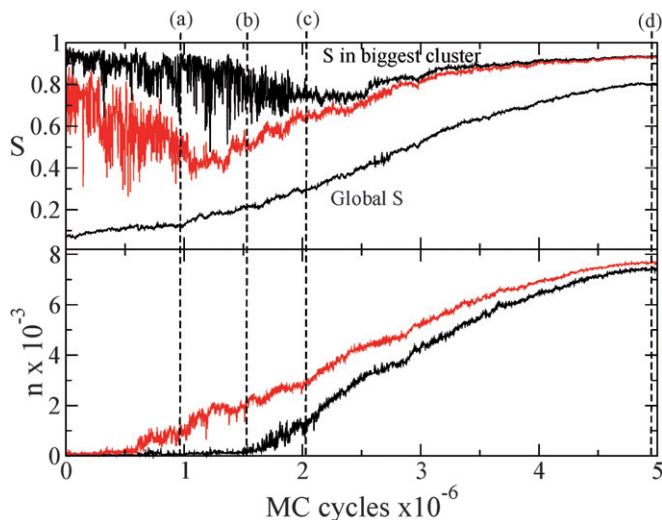


**Fig. 2** Evolution of the size of the biggest cluster  $n$  in the system (bottom panel), the nematic order parameter  $S$  of the biggest cluster and of the total system (top panel), for a HSC fluid with  $L^* = 3.4$  at  $P^* = 3.1$ . The black curves correspond to the results using the C2 cluster criterion, while the gray curves have been obtained using the C1 cluster criterion. The configurations corresponding to the snapshots of panels (a), (b), (c) and (d) of Fig. 1 are indicated with the vertical dashed lines.

with the C1 and the C2 cluster criterion. We find that the I–Sm transition is a two-step process. In the initial stage of the transition, many small clusters are formed throughout the whole system. These clusters are irregular, not very compact, and do have a smectic-like character, although it is hard to distinguish the smectic layers. Clusters with about 1–3 smectic layers are observed. We analyze a typical configuration in the initial stage of the phase separation according to both cluster criteria. The packing fraction of this configuration is  $\eta = 0.500$ , which is lower than the densest metastable isotropic fluid phase ( $\eta = 0.508$  at  $P^* = 3.0$ ). Fig. 1a and e, display the analysis according to the C2 and C1 criterion, respectively. Only a few tiny clusters are detected by the C2 cluster criterion (see Fig. 1a), while a much larger interconnected cluster is found by the less strict C1 criterion (see Fig. 1e). We find that the formation of a labyrinth-like, percolated, interconnected structure is detected in an earlier stage according to the C1 criterion than to the C2 criterion. We like to stress, that the clusters, even the smallest ones, do have a pronounced smectic-like character. This should be contrasted with the observations of Dogic and Fraden in suspensions of rod-like virus particles and non-adsorbing polymer. These authors observed that the transition to the smectic phase starts with the formation of nematic tactoids, and subsequently smectic layers are formed inside or on the surface of the tactoids. In a later stage of our simulations, the clusters grow, coalesce and form larger clusters, but also smaller clusters can diffuse away from the main cluster. As the clusters can have different orientations when they coalesce, the resulting cluster might have a nematic order parameter that is smaller than that of the original clusters. Again, we analyze a typical configuration with  $\eta = 0.515$  at this stage of the phase separation using both cluster criteria. Fig. 1b and f, display the analysis according to the C2 and C1 criterion, respectively. In this case, the C2 cluster criterion detects isolated clusters, while the C1 criterion finds an interconnected cluster. As the main mechanism for the growth of the clusters is by coalescence of smaller clusters at this stage, both the nematic order parameter and the size of the biggest cluster are very noisy and display huge sudden fluctuations. At a later stage, the

smectic clusters coalesce and form an interconnected cluster. This cluster is an open and branched structure, but with a clear smectic-like character as the smectic layers can clearly be distinguished in Fig. 1c. Finally, the size of the cluster grows by the addition of individual particles and the nematic order of the interconnected cluster grows gradually by reorientation of different parts of the cluster. Fig. 1d shows that eventually the whole system has been transformed into a structure of parallel stacks of rods, which are typical for the smectic phase. In conclusion, the observed phase separation process has all the typical features of spinodal decomposition: phase separation sets in immediately after compressing as many small clusters are formed throughout the system. These clusters coalesce to form an interconnected structure, which eventually transforms into the stable smectic bulk phase.

A similar kinetic pathway has been observed experimentally by Maeda and Maeda in a systematic study of the isotropic-to-smectic transition as a function of the particle elongation in  $\beta$ -FeOOH rod suspensions.<sup>10</sup> For rods with a length-to-width ratio of 3.5, they find at the beginning of the transition, the spontaneous formation of smectic clusters. When the density is increased the clusters grow laterally, coalesce on top of each other to form multilayer stacks until a single stable smectic structure is formed. A similar behavior has also been found for the isotropic-to-nematic transition in experimental<sup>11</sup> and computer simulation<sup>18,19</sup> studies at sufficiently high supersaturations.

At lower supersaturations ( $P^* \leq 3.0$ ) the system does not change spontaneously from the isotropic to the smectic phase, and we need umbrella sampling to study the transition. In this work, we study the I-Sm transition at supersaturations  $P^* = 2.828, 2.85, 2.90, 2.95$  and  $3.0$ , which correspond to metastable isotropic states with packing fractions  $\eta = 0.496, 0.498, 0.504$  and  $0.508 (\pm 0.001)$ , respectively. Before we discuss our results on the I-Sm transition, we wish to make a few comments on the structure of the metastable isotropic fluid phase. Visual inspection of typical configurations of the isotropic fluid shows that the fluid exhibits pronounced pre-smectic ordering as smectic-like groups of about 5–10 particles are already present in the isotropic bulk phase. A typical configuration at  $P^* = 2.9$  is shown in the inset of Fig. 3. The different colors reflect the different orientations of the rods. In addition, we also show the orientational pair correlation function  $g_2(r) = \langle P_2(\cos \theta(r)) \rangle$ <sup>21</sup> for various pressures, where  $r$  denotes the

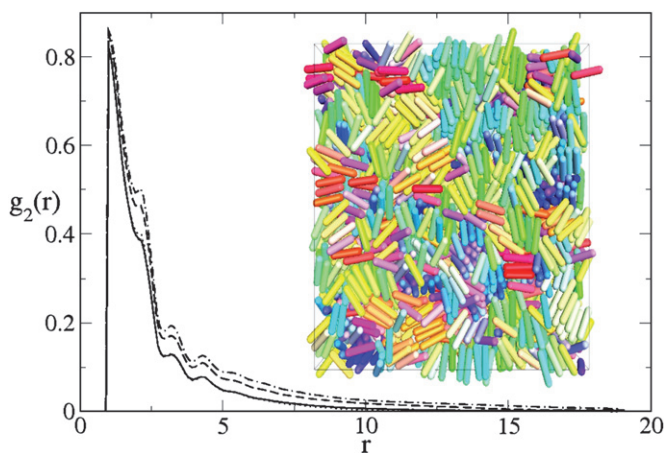
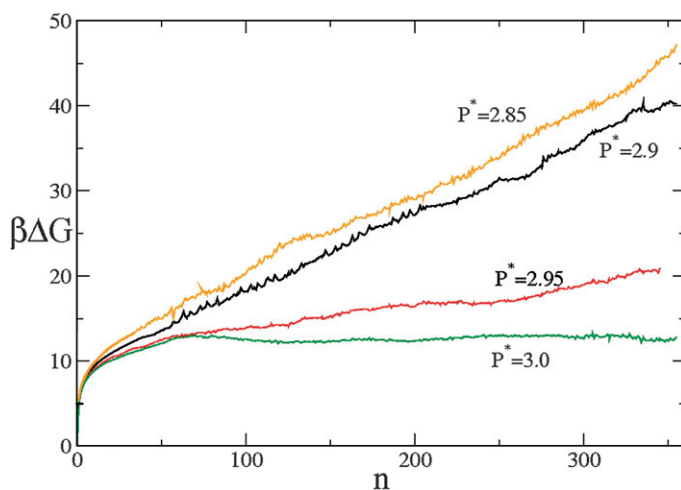


**Fig. 3** Orientational pair correlation function  $g_2(r)$  at coexistence pressure  $P^* = 2.828$  (solid line),  $P^* = 2.9$  (dotted line, coincides with the previous one),  $P^* = 2.95$  (dashed line) and  $P^* = 3.0$  (dotted-dashed line), where  $r$  denotes the center-of-mass distance between two particles in units of  $\sigma$ . The inset shows a typical isotropic configuration at  $P^* = 2.9$  with pronounced pre-smectic ordering, color is used to distinguish the different orientations of the particles.

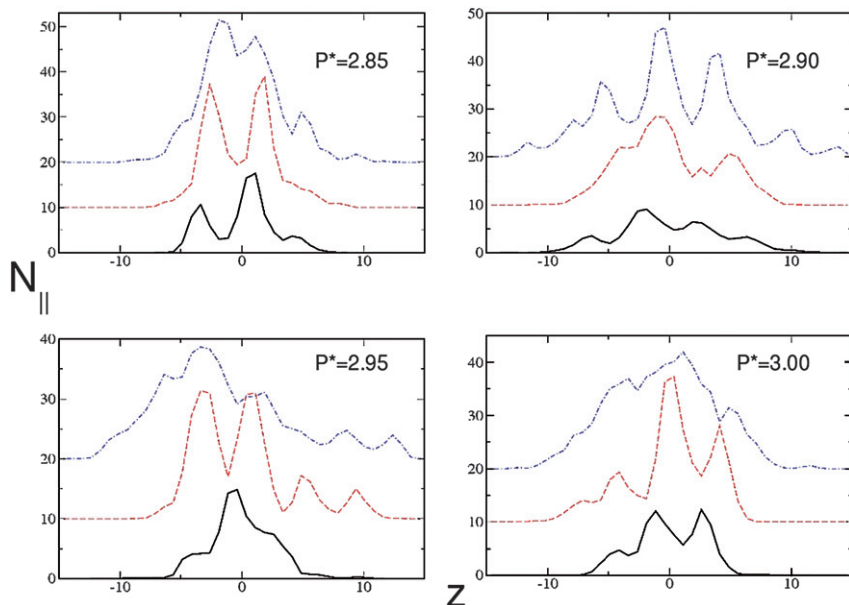
center-of-mass distance between the particles in units of  $\sigma$ . The orientational pair correlation function tends to zero at large distances as the orientational order vanishes at long-range as expected for the isotropic phase. On the other hand, we find strong orientational order at short distance, as can be observed from the pronounced peaks for small  $r$ , thereby providing evidence of the presence of small smectic-like clusters in the isotropic fluid phase. The peaks in the  $g_2(r)$  are at distances  $r \approx 1, 2$  and  $3$ , corresponding to the first, second and third neighbor in the same layer. The fourth peak appears at a distance  $r \approx 4.4$  corresponding to a particle in a different layer. The short-range orientational order becomes slightly stronger upon increasing the supersaturation. Fig. 3 shows the orientational pair correlation for the coexistence pressure  $P^* = 2.828$  and  $P^* = 2.9$ , which are indistinguishable from each other, and for  $P^* = 2.95$  and  $3.0$ . This short-range pre-smectic order may play an important role in the isotropic-to-smectic transformation, which we will study in the sequel of this paper.

We calculate the Gibbs free energy  $\beta\Delta G$  as a function of the number of particles  $n$  in the cluster using the umbrella sampling technique and the C2 cluster criterion. We did not use the C1 criterion in the umbrella sampling, as this criterion already detects huge clusters at the supersaturation of interest even if we do not introduce the bias in our sampling. However, we do use the C1 criterion to analyze our results. The free energy barriers are shown in Fig. 4 for  $P^* = 2.85, 2.90, 2.95$ , and  $3.00$ . We clearly observe from Fig. 4 that the free energy of formation grows linearly with the size of the cluster  $n$  without reaching a maximum for pressure  $P^* = 2.85, 2.90$  and  $2.95$ . For  $P^* = 3.0$ , we find that the free energy reaches a plateau or decreases slightly for  $n > 100$ .

Our results are very similar to the simulation studies of the isotropic-to-crystal nucleation of short hard rods of ref. 5,6 where the free energy also increases monotonically with cluster size. They attribute the absence of a nucleation barrier to self-poisoning of the crystallite by rods that lie parallel to the surface of the crystal clusters, thereby hindering the crystal growth. In order to study whether self-poisoning can explain our results, we study in more detail the structure of the smectic clusters and the surrounding particles of these clusters. We calculate the average number of particles  $N_{\parallel}$  as a function of the distance  $z$  from the center-of-mass of the cluster in the direction parallel to the nematic director for clusters with  $n = 100, 200$ ,



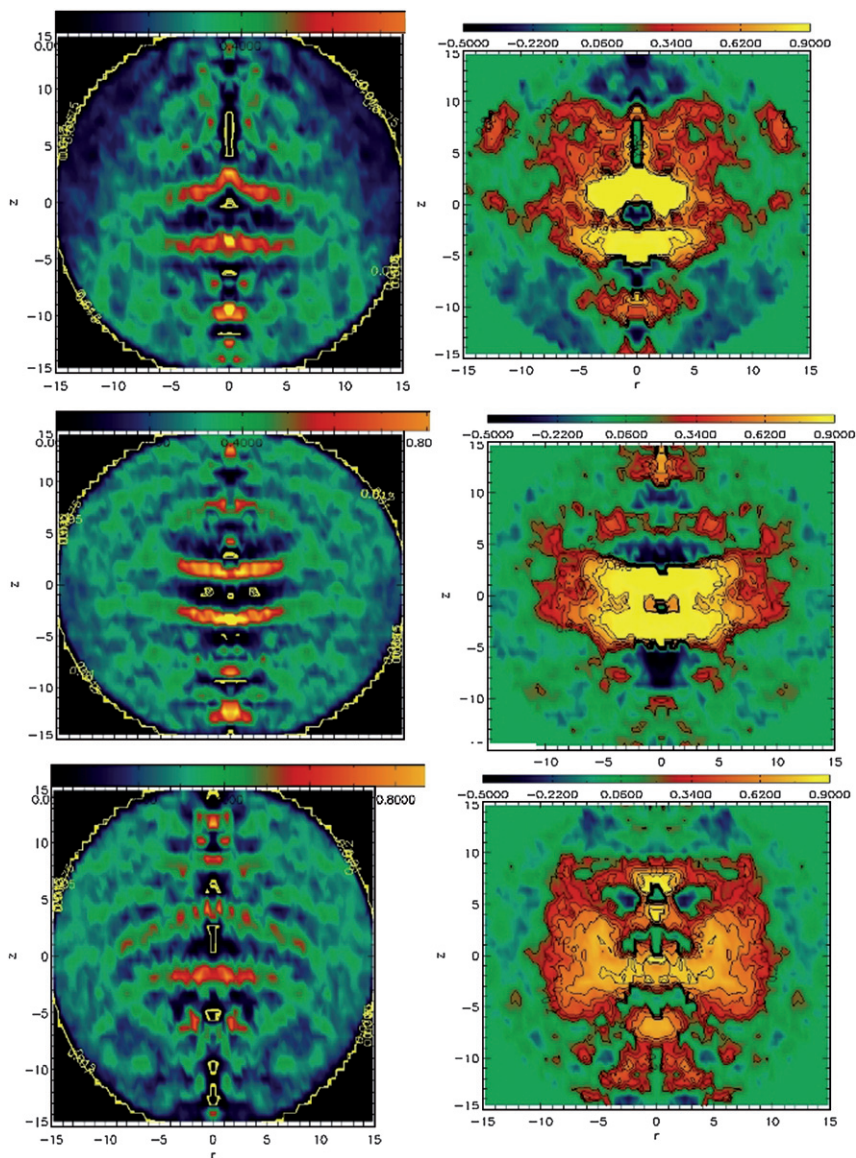
**Fig. 4** Gibbs free energy  $\beta\Delta G$  of a HSC fluid with  $L^* = 3.4$  as a function of the number of particles in the biggest cluster  $n$ , as calculated by umbrella sampling MC simulations using the C2 cluster criterion at pressures  $P^* = 2.85, 2.90, 2.95$  and  $3.00$ .



**Fig. 5** Averaged number of particles  $N_{||}$  as a function of the distance  $z$  from the center-of-mass of the cluster in the direction parallel to the nematic director for clusters with  $n = 100$  (black solid lines), 200 (red dashed lines), and 300 (blue dotted-dashed) particles at pressures  $P^* = 2.85, 2.90, 2.95$  and  $3.00$ . The unit of length is taken to be  $\sigma$ . Only the particles detected by the C2 cluster criterion have been considered.

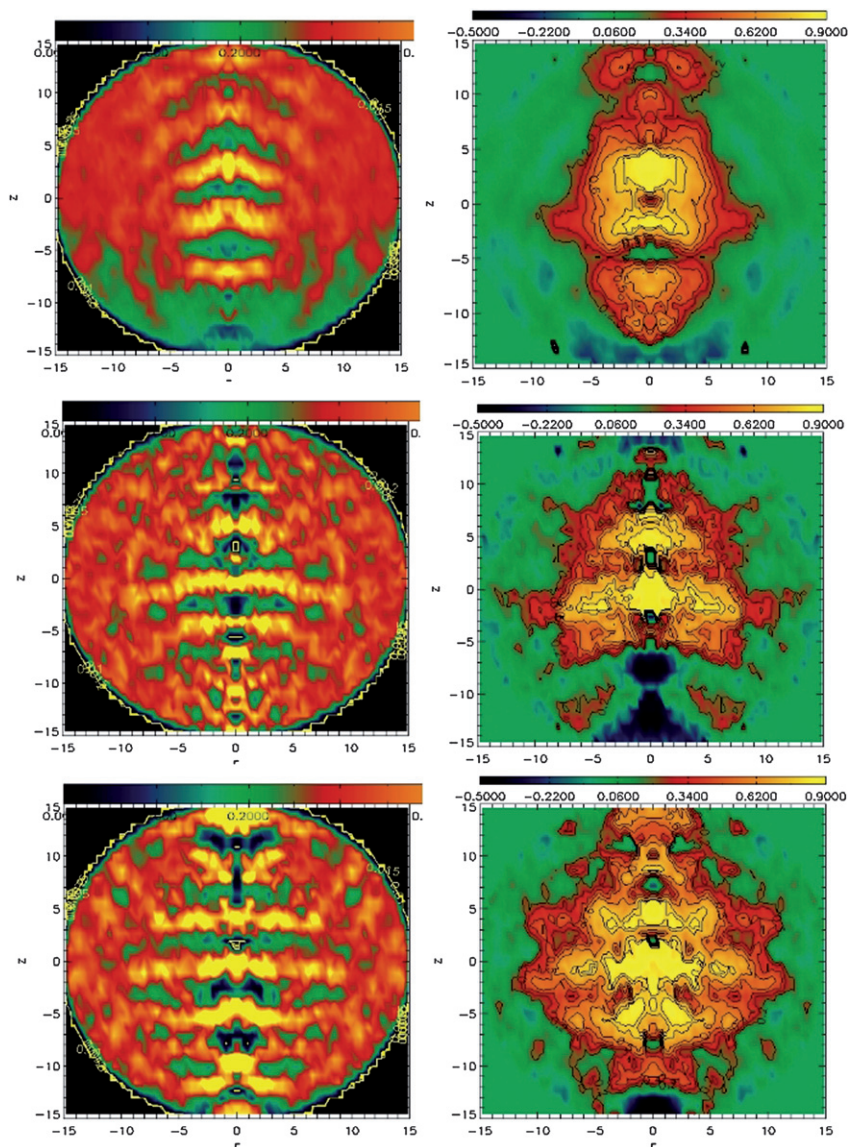
and 300 particles. The unit of length is taken to be  $\sigma$ . We only consider here the particles that are detected by the C2 cluster criterion. We show the results in Fig. 5 for  $P^* = 2.85, 2.90, 2.95$ , and  $3.00$ . Fig. 5 shows pronounced peaks in the number of particles, thereby providing clear evidence that the clusters consist of different layers. The distance between the peaks (and between the layers) is about  $L^* + 1$ , which is equal to the length of the rods and corresponds to the distance that one expects in the bulk smectic phase. Comparing Fig. 4 with Fig. 5 shows that there is no correlation between the number of layers and the Gibbs free energy. For example, we find very similar Gibbs free energy curves for  $P^* = 2.85$  and  $P^* = 2.90$ , but for  $P^* = 2.85$ , we find clusters of two layers for  $n = 200$  and 300, and three layers for  $n = 300$ , while for  $P^* = 2.90$  the number of layers ranges from four to six layers. Interestingly, we also find that the number of layers grows with the cluster size for all supersaturations. This should be contrasted with the results of ref. 5 where self-poisoning avoids the growth of additional layers to the cluster. Moreover, ref. 7 predicts a sequence of maxima and minima in the Gibbs free energy as a result of the nucleation of additional layers. Although we do find very weak oscillations in our Gibbs free energy curves, we were not able to find any correlations of the oscillations with the formation of additional layers to the cluster. We attribute the oscillations more to statistical fluctuations.

We also employ the umbrella sampling technique to study the shape and structure of the cluster as a function of its size. In Fig. 6, we show contour plots of the density profiles  $\rho(z, r)$  and nematic order parameter profiles  $S(z, r)$  for clusters of size  $n = 150, 250$  and  $350$  at  $P^* = 2.85$ . The contour plots at  $P^* = 2.9$  are shown in Fig. 7. Comparing Fig. 6 and 7, we find pronounced layering of the particles in the contour plots at both pressures. In the density profiles, we find layers with high density and nearly zero density in between the layers. As already observed in Fig. 5, we again find that the number of layers in the clusters is higher at  $P^* = 2.9$  than at  $P^* = 2.85$ .



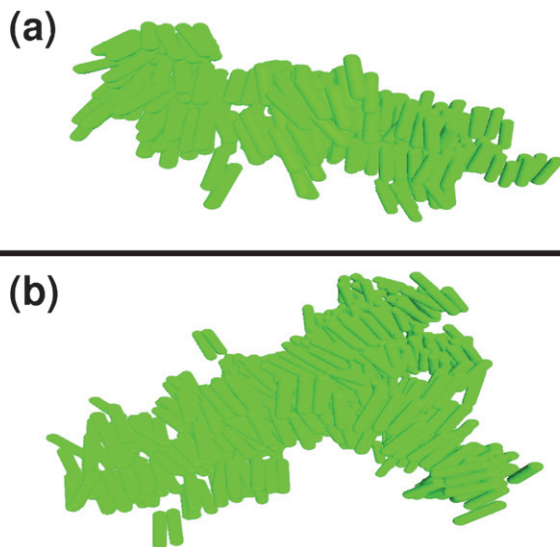
**Fig. 6** Contour plots for the density profiles  $\rho(z, r)$  (left) and nematic order parameter profiles  $S(z, r)$  (right) as a function of the distance from the center-of-mass of the cluster in the direction parallel ( $z$ ) and perpendicular ( $r$ ) to the nematic director for clusters of size  $n = 150$  (top),  $n = 250$  (middle) and  $n = 350$  (bottom) at  $P^* = 2.85$ . The unit of length is  $\sigma$ .

The nematic order parameter profiles show high orientational order in the cluster and hardly any orientational order outside the cluster. From the nematic order parameter contour plots, we also observe that the layers are almost perpendicular to the nematic director ( $z$  direction). Moreover, we also find evidence for particles that are aligned parallel to the top and bottom surface of the clusters, as the dark blue regions in the  $S(z, r)$  contour plots of Fig. 6 and 7 correspond to  $S(z, r) = -0.5$ . The observation of particles that are aligned parallel to the top and bottom surface of the clusters has also been observed in ref. 5.



**Fig. 7** Contour plots for the density profiles  $\rho(z, r)$  (left) and nematic order parameter profiles  $S(z, r)$  (right) as a function of the distance from the center-of-mass of the cluster in the direction parallel ( $z$ ) and perpendicular ( $r$ ) to the nematic director for clusters of size  $n = 150$  (top),  $n = 250$  (middle) and  $n = 350$  (bottom) at  $P^* = 2.9$ . The unit of length is  $\sigma$ .

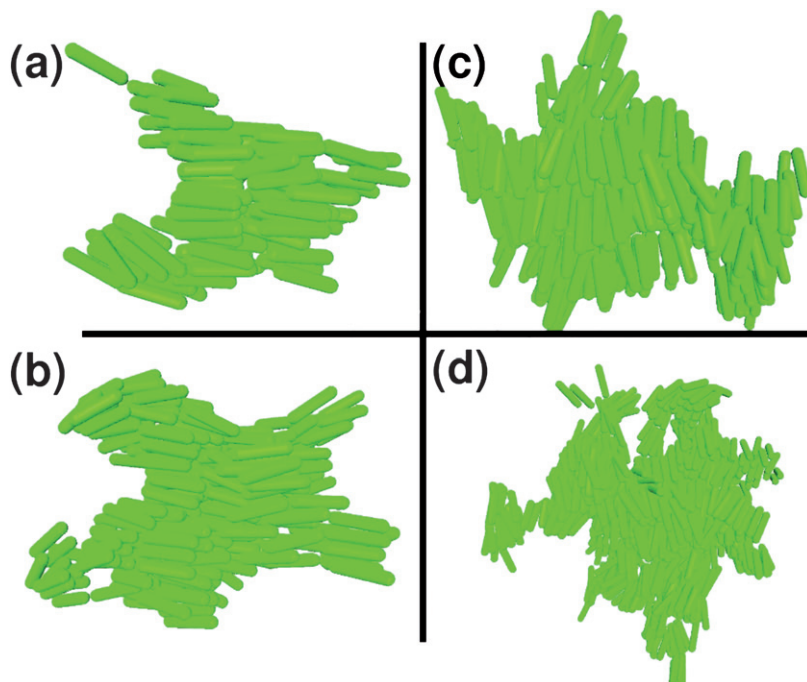
A closer inspection of Fig. 6 shows that we find isolated smectic clusters that are disconnected from the main cluster by a region of particles that are parallel to the surface of both clusters. These isolated smectic clusters can be observed for example in Fig. 6, for a cluster of size  $n = 150$  at  $z \approx -10$ , or at  $n = 250$  at  $z \approx 7, 13$  and  $-8$ . The isolated smectic clusters are also visible in, for instance, Fig. 9d. We already mentioned that the isotropic fluid phase shows pronounced pre-smectic ordering as small smectic-like clusters are already present in the isotropic phase. The isolated smectic clusters observed in Fig. 6 are probably the small smectic-like clusters that are already present in the isotropic fluid phase. Our simulations also show that



**Fig. 8** (a) A typical intermediate configuration in the I–Sm transformation of a HSC fluid with  $L^* = 3.4$  at  $P^* = 2.85$  analyzed with the C2 cluster criterion resulting in a cluster of 250 particles. (b) Same configuration as in (a), but analyzed by the C1 cluster criterion resulting in a cluster with 631 particles.

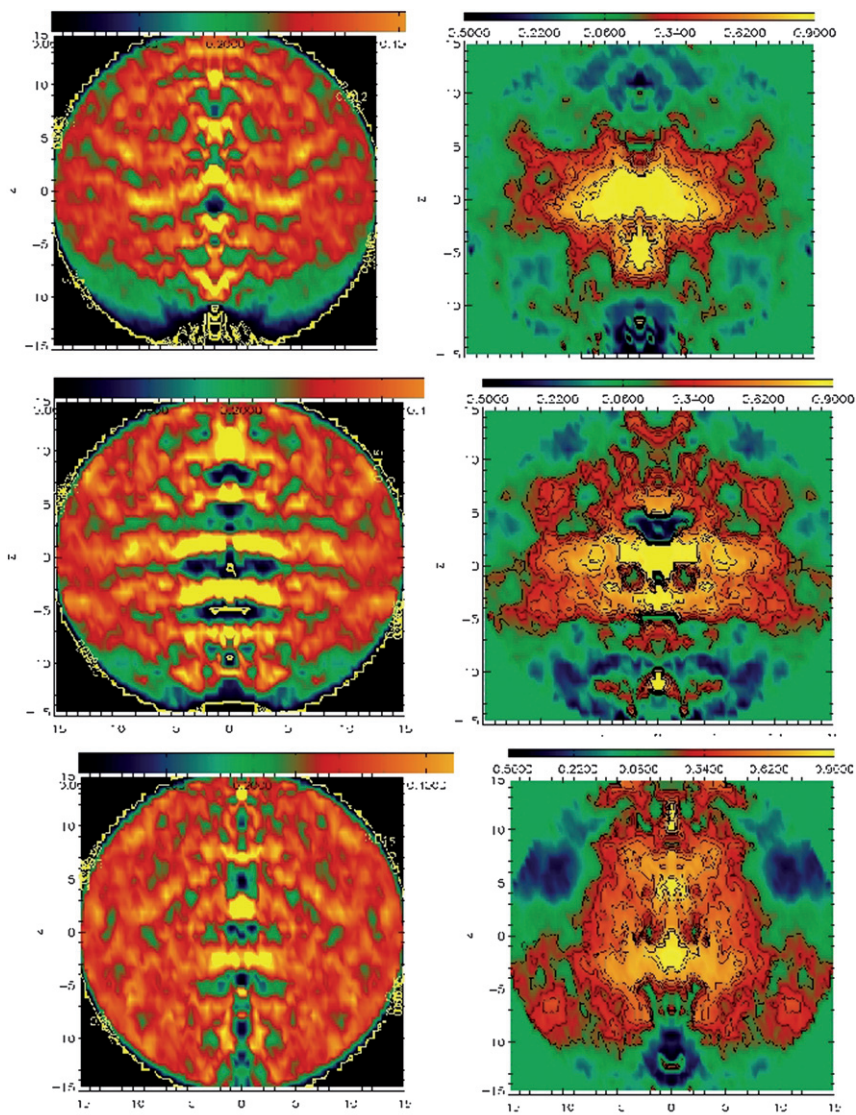
the growth of the clusters proceeds more by the reorientation and coalescence of small groups of particles than by individual particles. The growth of the clusters seems to be kinetically inhibited by the pre-smectic ordering, as the dynamics of the particles slows down because the particles can only diffuse by cooperative motion of the whole cluster.

We analyze typical configurations according to the C1 and C2 cluster criteria. Fig. 8 displays the analysis of a typical configuration at  $P^* = 2.85$ . We find that the C2 cluster criterion detects a cluster of 250 particles, while the less restrictive C1 cluster finds a cluster of 631 particles. In Fig. 9 we show typical configurations at  $P^* = 2.90$  analyzed with the C2 and C1 cluster criterion. The C2 cluster criterion detects clusters of 100 and 350 particles, respectively, while the C1 cluster criterion finds clusters of 221 and 846 particles. Again, the less restrictive C1 cluster criterion detects as expected clusters consisting of more particles. We also wish to note that the shape of the clusters can be very different. The clusters in Fig. 8 at  $P^* = 2.85$  are oblate, while the clusters in Fig. 9 are more prolate at  $P^* = 2.90$ . Fig. 5 also shows that the shape of the clusters can be very different and that there is no correlation between the cluster shape (or number of layers) and the supersaturation. According to classical nucleation theory, which is based on the assumption that the clusters are in quasi-equilibrium with the metastable parent phase, the Gibbs free energy  $\Delta G$  is given by a surface term and a bulk term. The bulk term is given by the volume of the cluster and the chemical potential difference between the phase inside the cluster and the supersaturated bulk phase. While the surface term for elongated particles depends on the interfacial tension, the anchoring strength and the surface and shape of the droplet. The “equilibrium” shape of the droplet can be determined by minimizing  $\Delta G$  with respect to the cluster shape for a given supersaturation and cluster size.<sup>17,19</sup> Our results show that there is no correlation between the shape of the cluster and the supersaturation and the size of the cluster. This might be explained by either the fact that the clusters are not in quasi-equilibrium or that the surface tensions of the droplets are extremely low. Hence, a theoretical description of the height and shape of the nucleation barrier by classical nucleation theory seems to be doomed to fail.



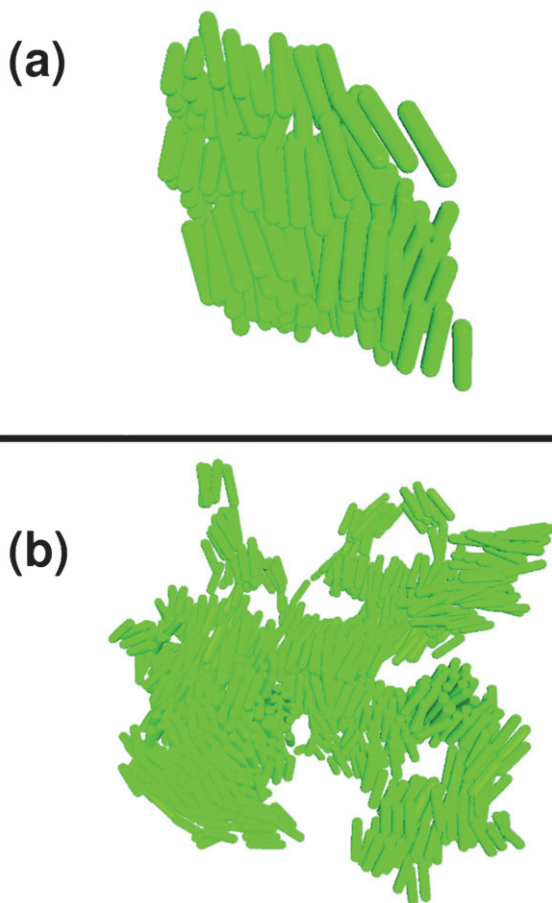
**Fig. 9** (a) A typical intermediate configuration in the I–Sm transformation of a HSC fluid with  $L^* = 3.4$  at  $P^* = 2.9$  analyzed with the C2 cluster criterion resulting in a cluster of 100 particles. (b) Same configuration as in (a), but analyzed with the C1 cluster criterion resulting in a cluster with 221 particles. (c) A typical intermediate configuration analyzed with the C2 cluster criterion resulting in a cluster of 350 particles. (d) Same configuration as in (c), but analyzed with the C1 cluster criterion resulting in a cluster with 846 particles.

Fig. 4 shows that the slope of  $\Delta G$  changes enormously if we change the supersaturation from  $P^* = 2.9$  to  $P^* = 2.95$ . We therefore study in more detail typical intermediate configurations at  $P^* = 2.95$  and 3.00. We first determine the contour plots of the density profiles  $\rho(z, r)$  and nematic order parameter profiles  $S(z, r)$  for clusters of size 150, 250, and 350. Fig. 10 presents the contour plots at  $P^* = 2.95$ . We again find similar features in the contour plots as at lower supersaturations. We again observe pronounced layering of the particles in the clusters and we also find particles that are parallel to the top and bottom surface of the clusters. Visual inspection of the cluster shows that the cluster is oblate at this supersaturation (not shown). We now analyze typical configurations using the C2 and C1 cluster criteria. Fig. 11 shows the analysis of a typical configuration at  $P^* = 3.00$ . The C2 cluster criterion detects a compact smectic cluster of three layers and with  $n = 200$  particles, while the C1 cluster criterion finds a very open interconnected labyrinth-like cluster of 1630 particles. The cluster detected by the C2 cluster criterion is located in one of the most ordered branches of the larger (almost percolating) network. The structure of this open network is still smectic-like as the individual smectic layers are clearly visible. However, the orientational order is not long-ranged as the layers can have different orientations in the network. The same observations can be made at  $P^* = 2.95$ . In conclusion, we find that at low supersaturation ( $P^* = 2.85$  and 2.95), a random cluster starts to grow in a metastable isotropic fluid phase. The shape and the number of layers of the cluster is determined by the chance to find a certain smectic cluster shape in a metastable isotropic fluid phase with pronounced pre-smectic ordering. At high supersaturations ( $P^* = 2.95$  and 3.00), we find that the metastable isotropic fluid phase shows a more pronounced pre-smectic ordering, where



**Fig. 10** Contour plots for the density profiles  $\rho(z, r)$  (left) and nematic order parameter profiles  $S(z, r)$  (right) as a function of the distance from the center-of-mass of the cluster in the direction parallel ( $z$ ) and perpendicular ( $r$ ) to the nematic director for clusters of size  $n = 150$  (top),  $n = 250$  (middle) and  $n = 350$  (bottom) at  $P^* = 2.95$ . The unit of length is  $\sigma$ .

smectic-like clusters merge together to form an interconnected network. The increase in pre-smectic ordering upon increasing the pressure results in a smaller slope of the free energy curves. The slope of the Gibbs free energy curve is nearly zero at  $P^* = 3.00$ . If we compress a well-equilibrated isotropic fluid phase to  $P^* = 2.95$  and 3.00, we find that the isotropic fluid phase is stable for more than  $10^6$  MC cycles, while phase separation sets in immediately when we quench the system to  $P^* = 3.1$ . We therefore conclude that state points  $P^* = 2.95$  and 3.00 are in the nucleation and growth regime, while  $P^* = 3.1$  is in the spinodal region. However, it is also possible that at  $P^* = 2.95$  and 3.00, the spinodal decomposition is kinetically inhibited as the system can only evolve by collective re-arrangements of the smectic



**Fig. 11** (a) A typical intermediate configuration in the I–Sm transformation of a HSC fluid with  $L^* = 3.4$  at  $P^* = 3.0$  analyzed with the C2 cluster criterion resulting in a cluster of 200 particles. (b) Same configuration as in (a), but analyzed with the C1 cluster criterion resulting in a cluster with 1630 particles.

domains, and that long equilibration times are needed to start the phase separation. It seems at odds that the system falls out-of-equilibrium at low supersaturation, where one would expect a faster dynamics of the individual particles, but this can be explained by the fact that collective rearrangements are favored at higher supersaturations.

#### 4 Conclusions and final remarks

In this paper, we have studied the isotropic-to-smectic transformation for a fluid of colloidal hard rods of length  $L^* = 3.4$  using computer simulations. We have found spinodal decomposition at high supersaturations, but we were not able to find a nucleation barrier for lower supersaturations as the free energy increases monotonically with cluster size. By analyzing the isotropic fluid phase, we find strong pre-smectic ordering as many smectic-like clusters are present at  $P^* = 2.85$  and  $2.9$ . At  $P^* = 2.95$  and  $3.0$ , we observe an open interconnected smectic-like network as the smectic clusters join together. More importantly, we also find that the shape of the intermediate structures can vary from oblate to prolate clusters and from 1 up

to 6 layers. As we do not find any correlation between the shape of the cluster and the supersaturation and cluster size, we conclude that the transient clusters are not in quasi-equilibrium with the parent phase as the shape of the clusters is not determined by an “equilibrium” shape of the cluster that can be derived by minimizing the Gibbs free energy as a function of the cluster shape. The cluster shape is more determined by the instantaneous pre-smectic structure of the isotropic fluid phase. We also find that the growth of the clusters proceeds more by the reorientation and coalescence of smectic-like groups than by individual particles as is usual for nucleation. Moreover, due to the pre-smectic ordering of the isotropic phase, the dynamics of individual particles is slow as diffusion can only occur cooperatively. We therefore conclude that the nucleation and growth of the smectic phase is hampered by the pronounced pre-smectic ordering in the isotropic fluid phase. Only when the collective rearrangements are favoured by a higher supersaturation, can we observe the I–SM transition, which occurs in a spinodal-like fashion.

One might think that the inclusion of attractive interactions, *e.g.*, depletion interactions induced by the addition of non-adsorbing polymer,<sup>22</sup> may help the nucleation of tactoids. However, a very recent study of our group has shown that the critical cluster for a system of attractive rods consists of a single layer that only grows laterally, while the nucleation of a second layer on top of the first layer is an extremely rare event.<sup>23</sup> Nucleation of multilayer clusters were never observed during the simulations.

## 5 Acknowledgements

This work is financially supported by a NWO-VICI grant and a TOP-CW funding of the “Nederlandse Organisatie voor Wetenschappelijk Onderzoek (NWO)” and by the High Potential Programme of Utrecht University. A.C. acknowledges support from *Juan de la Cierva* program of the Ministry of Science and Innovation of Spain.

## References

- 1 Z.-J. Wang, C. Valeriani and D. Frenkel, *J. Phys. Chem. B*, 2009, **113**, 3776.
- 2 P. R. ten Wolde and D. Frenkel, *J. Chem. Phys.*, 1998, **109**, 9901.
- 3 D. Moroni, P. R. ten Wolde and P. G. Bolhuis, *Phys. Rev. Lett.*, 2005, **94**, 235703.
- 4 E. Sanz, C. Valeriani, D. Frenkel and M. Dijkstra, *Phys. Rev. Lett.*, 2007, **99**, 055501.
- 5 T. Schilling and D. Frenkel, *Phys. Rev. Lett.*, 2004, **92**, 085505.
- 6 T. Schilling and D. Frenkel, *Comput. Phys. Commun.*, 2005, **169**, 117.
- 7 D. Frenkel and T. Schilling, *Phys. Rev. E*, 2002, **66**, 041606.
- 8 Z. Dogic and S. Fraden, *Philos. Trans. R. Soc. London, Ser. A*, 2001, **359**, 997.
- 9 Z. Dogic, *Phys. Rev. Lett.*, 2003, **91**, 165701.
- 10 H. Maeda and Y. Maeda, *Phys. Rev. Lett.*, 2003, **90**, 018303.
- 11 M. P. B. van Bruggen, J. K. G. Dhont and H. N. W. Lekkerkerker, *Macromolecules*, 1999, **32**, 2256.
- 12 P. Oakes, J. Viamontes and J. X. Tang, *Phys. Rev. E*, 2007, **75**, 061902.
- 13 M. P. Lettinga, K. Kang, P. Holmqvist, A. Imhof, D. Derks and J. K. G. Dhont, *Phys. Rev. E*, 2006, **73**, 011412.
- 14 Y.-G. Tao, W. K. Otter, J. K. G. Dhont and W. J. Briels, *J. Chem. Phys.*, 2006, **124**, 134906.
- 15 Z. X. Zhang and J. S. van Duijneveldt, *J. Chem. Phys.*, 2006, **124**, 154910.
- 16 J. Viamontes, P. Oakes and J. X. Tang, *Phys. Rev. Lett.*, 2006, **97**, 118103.
- 17 P. Prinsen and P. van der Schoot, *Phys. Rev. E*, 2003, **68**, 021701.
- 18 A. Cuetos and M. Dijkstra, *Phys. Rev. Lett.*, 2007, **98**, 095701.
- 19 A. Cuetos, R. van Roij and M. Dijkstra, *Soft Matter*, 2008, **4**, 757.
- 20 P. Bolhuis and D. Frenkel, *J. Chem. Phys.*, 1997, **106**, 666.
- 21 S. C. McGrother, D. C. Williamson and G. Jackson, *J. Chem. Phys.*, 1996, **104**, 6755.
- 22 S. V. Savenko and M. Dijkstra, *J. Chem. Phys.*, 2006, **124**, 234902.
- 23 A. Patti and M. Dijkstra, *Phys. Rev. Lett.*, 2009, **102**, 128301.